Title

Radio-enhancement by gold nanoparticles and their impact on water radiolysis for x-ray, proton and carbon-ion beams.

Journal

Physics in Medicine & Biology, 64(17)

Authors

Rudek, Benedikt
McNamara, Aimee
Ramos-Méndez, Jose
et al.

Publication Date

2019-08-28

DOI

10.1088/1361-6560/ab314c

Peer reviewed

HHS Public Access

Author manuscript

Phys Med Biol. Author manuscript; available in PMC 2024 July 04.

Published in final edited form as:

Phys Med Biol. ; 64(17): 175005. doi:10.1088/1361-6560/ab314c.

Radio-enhancement by gold nanoparticles and their impact on water radiolysis for x-ray, proton and carbon-ion beams

Benedikt Rudek,
Department of Radiation Oncology, Massachusetts General Hospital, Boston, USA; Department of Physics, Boston University, Boston, USA; Department of Ionizing Radiation, Physikalisch-Technische Bundesanstalt, Braunschweig, Germany

Aimee McNamara,
Department of Radiation Oncology, Massachusetts General Hospital, Boston, USA; Harvard Medical School, Boston, Massachusetts, USA

Jose Ramos-Méndez,
Department of Radiation Oncology, University of California San Francisco, San Francisco, USA

Hilary Byrne,
School of Physics, University of Sydney, Sydney, Australia

Zdenka Kuncic,
School of Physics and Sydney Nano Institute, University of Sydney, Sydney, Australia

Jan Schuemann
Department of Radiation Oncology, Massachusetts General Hospital, Boston, USA; Harvard Medical School, Boston, Massachusetts, USA

Abstract

Gold nanoparticle (GNP) radio-enhancement is a promising technique to increase the dose deposition in a tumor while sparing neighboring healthy tissue. Previous experimental studies showed effects on cell survival and tumor control for keV x-rays but surprisingly also for MV-photons, proton and carbon-ion beams. In a systematic study, we use the Monte Carlo simulation tool TOPAS-nBio to model the GNP radio-enhancement within a cell as a function of GNP concentration, size and clustering for a wide range of energies for photons, protons and, for the first time, carbon-ions. Moreover, we include water radiolysis, which has been recognized as a major pathway of GNP mediated radio-enhancement.

At a GNP concentration of 0.5% and a GNP diameter of 10 nm, the dose enhancement ratio was highest for 50 keV x-rays (1.36) and decreased in the orthovoltage (1.04 at 250 keV) and megavoltage range (1.01 at 1 MeV). The dose enhancement linearly increased with GNP concentration and decreased with GNP size and degree of clustering for all radiation modalities. While the highest physical dose enhancement at 5% concentrations was only 1.003 for 10 MeV protons and 1.004 for 100 MeV carbon-ions, we find the number of hydroxyl ($^{\bullet}OH$) altered by 23% and 3% after 1μs at low, clinically-relevant concentrations. For the same concentration

brudek@mgh.harvard.edu .

and proton-impact, the G-value is most sensitive to the nanoparticle size with 46 times more radical interactions at GNPs for 2 *nm* than for 50 *nm* GNP diameter within 1*μs*. Nanoparticle clustering was found to decrease the number of interactions at GNPs, e.g. for a cluster of 25 GNPs by a factor of 3.4. The changes in G-value correlate to the average distance between the chemical species and the GNPs. While the radiochemistry of GNP-loaded water has yet to be fully understood, this work offers a first relative quantification of radiolysis products for a broad parameter-set.

1. Introduction

Radiation therapy is used in treatment of cancer to deposit a lethal radiation dose in the tumor volume while minimizing the toxicity in the surrounding tissue. Due to their high probability of energy absorption and subsequent emission of short-ranged secondary electrons, high-atomic number materials such as gold (Z=79) have been suggested to locally sensitize tumors for radiation. Monte Carlo (MC) simulation codes are used to estimate this local dose enhancement on a nanoscopic scale [1].

While these simulations could explain the radio-enhancement of cells with the large physical dose enhancement of keV photons, the simulated *physical* enhancement in cells for protons was negligibly small [2] despite evidence of radio-enhancement in cell survival curves [3, 4, 5]. Carbon-ions have been used in only a few in-vitro experiments and nanoparticle mediated radio-enhancement has been observed but no simulation was presented to date [6]. As recent reviews on radio-enhancement by high-Z nanoparticles [7], and particular by gold nanoparticles (GNPs) [8], point out, chemical and biological mechanisms of gold nanoparticle radio-enhancement [9] need to be considered, too. Chemistry of water radiolysis has been implemented in MC simulation tools such as PARTRAC [10], Geant4-DNA [11], TRAXchem [12], KURBUCchem [13], RITRACKS [14] and TOPAS-nBio [15]. However, these implementations do not include any surface chemistry and experimental data on GNP mediated radiolysis is too incomplete and the processes too complex to allow an implementation in the foreseeable future. Experiments suggest that GNPs directly and indirectly enhanced reactive oxygen species (ROS) generation: they catalytically increase hydroxyl ($^{\bullet}OH$) and superoxide (O_2^-) production in water [16, 17, 18], bind ROS scavengers inside cells [19] and inhibit regulation of redox reactions [20]. The hydroxyl production enhancement is, however, complex and depends on GNP concentration, radiation dose and linear energy transfer (LET) [21]. At high doses, GNPs may also protect from oxidative damage via hydrogen peroxide (H_2O_2) decomposition and superoxide scavenging [22]. Disregarding any catalytic behavior, simulation studies focus on the species production by secondary electrons. A first simulation study on chemical enhancement around a single GNP using an early version of Geant4-DNA chemistry found enhanced radiolysis that varies as a function of distance from the nanoparticle surface and of proton energy [23]. The production of radical species was proportional to production of secondaries as previously observed in pure water [10].

In this paper, we extend previous studies by simulating the physical dose enhancement of GNPs as a function of GNP concentration, GNP size and clustering for a wide range of

energies for photons, protons and carbon-ions. Then we compare physical enhancement to changes in the number of chemical species produced in the presence of randomly distributed, isolated and clustered GNPs in a simple spherical cell model.

2. Material and Methods

The simulations were performed using the TOPAS-nBio extension [24, 25] of the TOPAS [26] Monte Carlo system version 3.1.p3. This TOPAS release is based on Geant4 version 10.3.p1 [27]. Both, the physical and chemical stage were simulated to estimate the impact of GNPs on energy deposition and free radical production.

2.1. Geometry

Two concentric water spheres were used to represent a simple cell geometry. The outer sphere with a diameter of 9 μm modeled the cytoplasm and contained a sphere of 5.4 μm diameter as the nucleus. It is the same ratio as used by Lin et al. for breast cancer cells but with a 1.5 times smaller scale [21]. The cell was centered in a cubic water box of 12 μm side length. Cell volumes show a large variability and when assumed to be spherical their diameter ranges from 2 μm to 200 μm. The size was chosen to be large enough to absorb secondary electrons created within the volume and as small as possible to reduce computation time. Following this argument, the geometry for the proton and carbon-ion simulations was ten times smaller than for photons. The shape of the GNPs was chosen to be spherical for which the highest uptake is expected [28]. GNPs were placed in the cytoplasm only, because GPNs predominantly enter a cell by endocytosis and are clustered within vesicles and other organelles within the cytoplasm [29]. The number of GNPs within a cluster and the distance between them was independently defined in the parameter file.

The GNP diameter ranged from 2 nm to 50 nm which showed the highest uptake in cell experiments [30, 31, 32]. The GNP concentration was defined as the weight of all GNPs inside the cytoplasm divided by the weight of the cell and was varied between 0.001% and 5% for photons and between 0.01% and 50% for protons and carbon-ions. Table 1 summarizes the number of GNPs inside the cytoplasm for each weight concentration and the corresponding concentration in units of mg/ml and μM. Figure 1 shows the cell geometry for isolated and clustered GNPs of 10 nm diameter at a concentration of 5% in weight.

The radiation was chosen to be monoenergetic, plane-parallel, to have the same diameter as the cytoplasm and to start 1.5 μm and 150 nm upstream of the cell model for the large and small cell, respectively. Large distances would lead to secondary electron build-up, and scattered electrons could laterally escape the region of interest and thereby falsely increase the dose enhancement [33]. Electron contributions, spectral broadening and beam attenuation influence the absolute dose under experimental condition but cancel within this relative parameter study.

2.2. Physical stage

Physical interactions within Geant4 are defined in the so-called physics list that describe processes and models in defined energy limits and materials. The most detailed track-structure physics list at very low energies for liquid water is Geant4-DNA [27] that tracks

electron interactions down to an thermalization energy of 7.4 eV in the default option, including vibrational and electronic transitions in liquid water. We used the default Geant4-DNA for the simulation of particle transport within the cell but Geant4-DNA currently does not include cross sections for gold. Thus, we used the Livermore physics list with 10 eV secondary electron production threshold [34, 35] and the recently implemented full Auger deexcitation cascade process [36] to model fluorescence, Auger electron production, and particle induced x-ray emission. The range cut for electrons was set to 1 nm and the tracking step-size to half the GNP radius. The simulated energy range was from 50 keV to 1 MeV for photons, from 1 MeV to 100 MeV for protons, and 10 MeV to 1000 MeV for carbon-ions. The mean dose enhancement was defined as the ratio of the dose scored to the medium of interest (i.e. the nucleus, cytoplasm or water box) in the presence of GNPs to that with the GNPs replaced by equivalent volumes of water (water nanoparticles (WNPs)). Due to the differences in the physics lists it was important to simulate these water nano-volumes with the Livermore physics list used for the GNPs instead of Geant4-DNA used in the other water volumes.

2.3. Chemical stage

The radiolysis of water following the initial ionization and excitation processes was simulated using a recent implementation of chemical processes in the TOPAS-nBio extension [15] which facilitates the use of the Geant4-DNA chemistry module. The revised reaction diffusion coefficients and reaction rate constants for solvated (aqueous) electrons (e^-_{aq}), hydroxyl ($^\bullet OH$), hydrogen ($H^\bullet$), dihydrogen (H_2), hydroxide (OH^-) and hydrogen peroxide (H_2O_2) as summarized by Ramos-Mendez et al. [15] were used. In the prechemical stage, the excited ($H_2O^\bullet$) and ionized (H_2O^+) water molecules dissociate to generate the initial species $^\bullet OH$, $H^\bullet$ and e^-_{aq}. After 1 ps the chemical stage starts in which these species diffuse freely through the water volume by Brownian motion and react following a totally-diffusion controlled approach. After 1 μs all reactive species have diffused sufficiently far that further reactions among them are unlikely. Reactions with other solutes in the cellular environment that can happen at any time are not included in the simulation. All MC codes currently only consider radiolysis in a pure water environment at neutral pH and 25°C and in this work chemical species are stopped and killed when they hit a GNP.

The time-dependent G-values (chemical species per 100 eV of deposited energy) and the number of radical species terminated at the GNPs per picosecond were calculated for photons, protons and carbon ions in pure water, for a GNP concentration of 0.5% in the cytoplasm and for various GNP parameters.

The material balance equation between reducing and oxidizing species was satisfied within 1% for pure water simulated with the Geant4-DNA physics list. However, the G-value for hydrated electrons was about 10% too low when the Livermore physics list was set as default with Geant4-DNA physics used in water regions as in Figure 5. This discrepancy is due to the interference of the two lists and will be solved in the upcoming Geant4-DNA release where the implementation of gold cross sections will supersede the use of physics lists in regions. For calculation of the average distance between radicals and GNPs (table 2), it was assumed that equidistant GNPs are surrounded by spherical volumes of water.

With the radius of these water sphere $r_{watersphere}$ the average distance of uniform-randomly distributed species from a GNP is then calculated as $(r_{watersphere} - r_{NP})/2$. With the diffusion constant D, time τ and distance traveled λ, the minimum time (straight line, no jitter) is $\tau = \lambda^2/(6 \cdot D)$.

3. Simulation results

3.1. Physical stage

3.1.1. GNP Concentration—Figure 2 shows electron emission spectra at the gold surface and corresponding dose enhancement in the cytoplasm and nucleus as a function of GNP concentration for a set of photon, proton and carbon-ion energies. The GNP size is 10 nm in diameter and GNPs are distributed randomly within the cytoplasm.

The electron spectra scored at the surface of a 10 nm GNP in figure 2a) show a strong contribution from Auger electrons around 2 keV, that follow photo-ionization of the M-shell. A low energy tail below 2 keV is created by the ionization of delta electrons and energy loss of the Auger, Compton and photo-electrons as they escape the GNP bulk to the surface. The electron range R in liquid water is around 10 nm for energies from 1 eV to 1 keV and the range for larger energies can be described by $R(E[eV]) = 0.0535 \cdot E^{1.706} \mu m$ [1, 37] i.e. 3 μm for 10 keV and 150 μm for 100 keV. Because electrons below 2 keV do not reach the nucleus, the enhancement in the nucleus is at least a factor of two lower than in the cytoplasm. This factor is 2.6 for 50 keV and only 2.0 for 100 keV photons due to the contributions of K-shell photo electrons at 19.3 keV and KLL Auger electrons above 52 keV. For all radiation modalities, the dose enhancement increases linearly with the GNP concentration. Its maximum is 4.63 for 50 keV photons which is a typical peak-energy for inter-operative x-ray sources, and decreases with photon energy.

The electron emission spectra in figure 2b) and c) for proton and carbon-ion impact compare spectra for a GNP and WNP (light colors, dotted lines). The fall-off at high electron energies marks the maximum energy transfer to electrons which is 2.2 keV, 21.8 keV, 54.5 keV and 109.9 keV for 10 MeV, 25 MeV, 50 MeV and 75 MeV protons, and 1.8 keV, 18.2 keV and 182.5 keV for 10 MeV, 100 MeV and 1000 MeV carbon-ions. While the number of emitted electrons is about 28 times larger for 10 MeV carbon-ions than 1 MeV protons correlating with the 27 times higher LET (673.0 keV/μm vs 26.2 keV/μm), the ratio between number of emitted electrons for a GNP and WNP is about 2:1 at 10 eV and 10:1 at 800 eV for both modalities, so that a similar dose enhancement is to be expected and observed in figure 2e) and f). The maximum dose enhancement for 10 MeV for protons and 100 MeV for carbon ions is 1.34, and 1.39, respectively, at GNP concentrations of 5%. Unlike for photons, the dose enhancement in the cytoplasm is relatively independent of the proton energy above 10 MeV as pointed out in previous work [38, 39]. It decreases by about 20% for 1 MeV protons, because the ratio of total emitted electron energy by a GNP and by a WNP is around 6.3 for proton energies of 10 MeV and above but only 5.1 for 1 MeV protons. The dose enhancement in the nucleus is about one third less than in the cytoplasm for proton energies above 1 MeV. The range of secondary electrons generated by 1 MeV protons is too

low to induce dose enhancement in the nucleus. For proton energies of 10 MeV and above the dose enhancement in the nucleus amounts to only 0.2% at 5% gold concentration.

3.1.2. GNP Clustering—Dose enhancement as a function of cluster size is shown in figure 3. The GNP diameter is 10 nm and the concentration in weight is 0.5% for photons. The concentration for simulations with protons and carbon-ions is increased to 5% as only a small enhancement is expected. Dose enhancement in the cytoplasm is reduced from 1.36 to 1.33 when the GNPs irradiated with 50 keV photons form clusters of 25 particles. For the other photon energies, the change is from 1.25 to 1.24 at 100 keV, from 1.04 to 1.03 at 250 keV, and from 1.012 to 1.000 at 100 keV. The change in the nucleus is negligible. The enhancement is up to two orders of magnitude lower for protons and carbon-ions which makes the data appear more noisy. The decrease in the mean dose enhancement from isolated GNPs to clustered GNPs (clusters of 25) is between 10% and 22%, however with large uncertainties.

3.1.3. GNP Size—The dose enhancement for GNPs between 2 nm (5 nm for photons) and 50 nm diameter is shown in figure 4 for a fixed concentration of 0.5% for photons and 5% for protons and carbon-ions. The enhancement decreases with GNP size as self-absorption becomes more likely. The low dose enhancement for 2 nm GNPs shown for proton and carbon-ion irradiation is an artifact created by the 1 nm tracking step length and 1 nm range cut-off in the simulation [35]. The trend in dose enhancement with increase in cluster size is comparable to the trend with the increase in size of a single GNP. A cluster of 25 10 nm-large GNPs has a slightly smaller weight ($2.53 \cdot 10^{-19}$ kg) than a single 30 nm GNP ($2.73 \cdot 10^{-19}$ kg) but a slightly larger dose enhancement, e.g. 33.0% vs 31.3% for 50 keV photons, because the cluster is less densely packed than a larger GNP.

3.2. Chemical stage

Figure 5a), b) and c) shows the G-values as a function of time for seven radical species for the three radiation types at energies of their highest physical dose enhancement, namely 50 keV for photons, 10 MeV for protons and 100 MeV for carbon-ions. The results are obtained for the small cell model filled with water and compared to the same model containing 0.5% GNP of 10 nm diameter in the cytoplasm in figure 5d), e) and f). The radicals are terminated at the GNPs within the simulation as if the GNPs were radical-scavengers so that the G-value is reduced once a radical hits a GNP. The number of radical species hitting a GNP per picosecond is plotted in figure 5g), h) and i) and normalized on the number of incident particles and binsize. As the statistics increase at later times with larger binsize, the error bars become smaller.

Hydroxyl ($^{\bullet}OH$), solvated electrons (e^{-}_{aq}) and hydronium (H_3O^{+}) are most abundant at 1 ps after the prechemical phase and their G-value decreases in the chemical phase while the G-value of hydrogen peroxide (H_2O_2), hydroxide (OH^{-}) and molecular hydrogen (H_2) increases as product of reactions between the radical species. The initial G-values are similar for all three modalities and change in comparable amount for photon and proton beams but show more pronounced changes for the carbon-ion beam. The LET in water for the 100 MeV carbon-ion beam is 172.1 keV/μ compared to 4.6 keV/μ for 10 MeV protons so that

the changes over time are more pronounced as chemical reactions between radicals are more likely for densely ionizing radiation.

The presence of GNPs (simulated as radical scavengers) reduces the total sum of G-values at 1 ps by about 15%, changes the ratio between G-values of different species and causes a faster decrease in G-value over time. In particular, the G-values for the most abundant radicals e_{aq}^{-}, H_3O^+, and $^{\bullet}OH$ decline (by about 35%, 30% and 15%) but they initially increase for H, H_2, H_2O_2 and OH^- (by about 43%, 74%, 244% and 236%; values are in the same order for the three modalities and averaged). These changes are either induced by a redistribution of energy deposition, by the radicals not produced in regions occupied by GNPs, by radicals being terminated at GNP surfaces or by their reaction partners missing after termination. The number of precursor molecules (e_{aq}^{-}), $H_2O^{\bullet}$ and (H_2O^+) have been calculated to be independent of all GNP parameters for particle beams (data not shown), as the dose enhancement at, for instance, 10% GNP concentration is only 0.6% and counteracted by a missing water volume of 0.5% now occupied by GNPs.

The number of radicals hitting GNPs per unit time displayed on double-logarithmic scale in figure 5g), h) and i) show that H_3O^+ which has the highest diffusion coefficient [15] most often interacts with a GNP and is terminated in the simulation. The graphs 5g), h) and i) show changes in slope indicating whether the radical was created at the prechemical phase or at a later time by chemical reactions. The changes are larges for the carbon-ion which has the highest LET. The scale of each y-axis in figure 5g), h) and i) spans the same order of magnitudes for comparison of the slops but note that the scale is five orders of magnitude lower for incident photons in figure 5g) than for the particle beams.

Figure 6 analyzes the influence of GNP-distribution and beam parameters on the hydroxyl production which is qualitatively similar for all seven species. Unless otherwise stated, the parameter set comprises a 10 MeV proton beam, 0.5% GNP concentration and 10 nm GNP diameter. The dotted blue line serves as reference depicting the G-value of hydroxyl calculated in the pure water cell.

The concentration dependence in figure 6a) shows the G-value of hydroxyl to decrease at a weight concentration of only 0.1%. This decrease saturates at 0.5%. The concentration dependence in figure 6d) shows an exponential decline in the $OH^{\bullet}$ count. The integrated number of $OH^{\bullet}$ within 1 μs is given in the brackets within the figure legends. For the lowest concentration of 0.01% only every tenth $OH^{\bullet}$ per incident proton is hitting a GNP, one $OH^{\bullet}$ for a concentration of 0.1% and this number is linearly increasing with concentration up to 1%, then leveling off which indicates that reactions between radical species are disturbed by the termination at the GNPs.

As the cluster size increases, the impact of nanoparticles decreases and the G-value moves closer to the reference line (figure 6b)). Figure 6e) shows that the number of $OH^{\bullet}$ terminated at GNPs just changes after 1 ns with less $OH^{\bullet}$ being terminated the larger the cluster is.

The changes introduced by smaller GNP sizes shown in figure 6c) and f) are qualitatively similar to an increase in concentration: more $OH^{\bullet}$ hit the GNPs and the two changes in slope move to earlier time points. For smaller GNP sizes the GNPs are more densely distributed

at fixed concentration of 0.5%. The G-value is even below the saturation level shown for the concentration dependence in figure 5c) because species are more densely distributed and less likely to escape cytoplasm without interaction with a GNP.

In table 2, the average distance $OH^{\bullet}$ diffuses until it hits a nanoparticle, the diffusion time in ns and total surface area of the GNPs is compared. The mean diffusion distance of $OH^{\bullet}$ in water is about 100 nm after 1 μs [15]. The change in G-value is partly a surface area effect, but an enhanced surface cannot fully account for the change: for 10 nm GNPs, a concentration of 2.5% has the same surface area as 2 nm GNPs at a concentration of 0.5%. The G-value for the smaller GNP size is much smaller better correlating to the almost three times smaller distance between radicals and GNPs.

4. Discussion

4.1. Physical stage

The physical dose enhancement is summarized in table 3 for a GNP concentration of 0.5% for photons and 5% for particle beams. Clinically relevant nanoparticle concentrations range from 0.001% to about 1% in weight for therapeutic applications and up to 5% for diagnostic imaging [7]. The ratio of the mass energy absorption coefficient μ_{en}/ρ [40] of the gold-water mixture and pure water is a rough estimate that underestimates the dose enhancement. The high keV x-ray dose enhancement is due to the z^3 dependence in the photo ionization cross section that leads to a more than two orders of magnitude higher cross section for gold compared to water at 50 keV [41].

The electron emission cross section for ion-impact, on the other hand, only depends on the target parameter via the electron binding energy and the electron velocity [42] which are in the same order of magnitude for gold and water. The observed dose enhancement for particle beams is, hence, negligible small. Very localized (within 10 nm) dose enhancement around 4 nm GNPs has previously been attributed to electrons from Auger cascades [43] from M-shell electrons but was not observed at larger diameters of 10 nm as used here or 100 nm presented in reference [36] because low-energy Auger electrons are absorbed in larger GNPs. Simulations for proton impact on larger cell geometries with biological endpoints such as strand breaks in the nucleus [2] and corresponding cell survival [38] found little or no effect of GNPs in proton irradiation and concluded that the number of protons in a 2 Gy irradiation that hits a GNP and induces electron emission with a range higher than 100 nm is negligibly small [2].

Note, however, that Geant4 uses Bethe-Bloch theory to describe electrons emission from proton and carbon ionization with emission only above the mean ionization potential of the medium. This potential is 78 eV for water and 790 eV for gold (excluding K and L shell) which correlate to the peaks in figure 2b) and c). Lower electron energies stem from delta electrons generated via ionization from proton and carbon-ion induced electron transport. This limitation leads to an underestimation of radio-enhancement within the first 10 nm of a GNP irradiated by proton and carbon-ion beams. An discretized ionization model based on cross sections calculated in the Binary Encounter Approximation as used in TRAX showed an increase of low-energy electron emission (¡1 keV) of up to two orders of magnitude [44]

which would increase the dose enhancement. Substituting the condensed-history models for electron transport with discrete models would further improve the accuracy of the simulation [34, 45].

Clustering leads to overlapping of radial dose distributions of neighboring GNPs that alters the dose enhancement on a nano- and a micro-scale. Dependent on the cluster size, geometry and morphology [46] and the angular emission pattern under photon [47] and electron [45] irradiation, nanoscopic hot-spots are formed between GNPs and in the periphery of the cluster. Outside the cluster, however, electron absorption in neighboring GNPs reduces the energy deposition of individual GNPs and the total dose enhancement of the GNP ensemble is decreased. In a dense hexagonal close packing cluster of 91 GNPs, the dose deposition of the center GNP was found to be reduced by 29% and that of a peripheral GNP by 2% [48]. The degree of this reduction depends on the solid angle that is shaded by neighboring GNPs and by the range and angular distribution of the emitted electrons. The effect on the dose enhancement in the cytoplasm amounted to only few percent in the presented simulations. Absorption in gold was found to be more pronounced as a function of GNP diameter and agrees with previously reported increased self-absorption for larger diameters [49] and subsequently reduced dose deposition per ionization [38].

4.2. Chemical stage

The impact of multiple GNPs on radiolysis has been simulated for the first time. In the current implementation in TOPAS-nBio the chemistry reactions are valid only for water. Thus, the radical species are stopped at any material other than water so that the G-value for the GNP-loaded cell is calculated to decrease as a function of GNP concentration. The lack of reactions to describe the behavior at GNP surfaces produces results that indeed contradict experimental findings of increased production for hydroxyl ($^{\bullet}OH$), superoxide (O_2^-), and hydrated electrons [16, 17, 18, 50]. However, the relative deviation from the reference G-value of a pure water model can help to quantify the influence of various nanoparticle parameters such as concentration, size and clustering. Moreover, we show in figures 5g), h) and i) the number radical species hitting the GNPs for photon, proton and carbon-ion beams, and in figures 6d), e) and f) the number of hydroxyl radicals $OH^{\bullet}$ hitting the GNPs as a function of these GNP parameters. These numbers can be folded with experimentally observed reactions to estimate realistic changes in the G-value - resulting most often in an increase.

The simulated changes in G-value for the three radiation modalities are similar in form and order of magnitude which may be surprising given the large differences in physical dose enhancement. Note, however, that dose enhancement is based on the differences in the interaction cross sections of gold and water, whereas the G-value describes the production of radicals upon energy deposition. The G-value depends on the electron spectra and the spatial distribution of radical production. The electron spectra shown in figure 2a) 50 keV photons, b) 10 MeV protons and c) 100 MeV carbon-ions share a long tail of low energy electrons and a similar maximum energy of 35.6 keV for photo-electrons, 21.8 keV for proton-impact and 18.2 keV for carbon-ion impact. The G-value for 100 MeV carbon-ions sticks out due to the dense distribution of radicals in the high LET beam of 172.1 $keV/\mu m$ compared

to 4.6 $keV/\mu m$ for 10 MeV protons (for a discussion of LET dependence see figure 6 in reference [15]). The saturating number of radical interactions at GNPs for increasing GNP concentration shown in figure 6d) and increased number of interaction for smaller particle size shown in figure 6f) agrees qualitatively with experimental findings by Cheng et al. [51]. Clustering reduces the number of interactions at GNPs (figure 6e)) as the available GNP surface decreases and the distance between radicals and GNPs increases. Dose hot-spots in GNP cluster as origin of radical species as hypothesized by Gandoue et al. [46] would locally increase the radical density, which would have limited impact for cluster in vesicles [29] but would increase damage for GNP-surrounded organelles such as mitochondria [52]. The key point comparing physical and chemical "enhancement" by GNPs is that GNPs directly interact with the primary particle for physical enhancement, whereas GNPs can interact with any radical species created in water within the diffusion distance.

5. Conclusion

The TOPAS-nBio Monte-Carlo simulation tool to was used to systematically investigate the dose enhancement by gold nanoparticles as a function of GNP concentration, size and clustering for a wide range of energies for photons, protons and carbon-ions. All GNPs were placed in the cytoplasm of a two-sphere cell model and the dose deposition in the cytoplasm and nucleus was scored for GNPs and WNPs to calculate the dose enhancement. The dose enhancement linearly increased with GNP concentration and decreased with GNP size and degree of clustering for all radiation modalities. The enhancement ratio was 1.36 for 50 keV, 1.24 for 100 keV, 1.04 for 250 keV and 1.01 at 1 MeV x-ray energies for a GNP concentration of 0.5% in weight and a GNP diameter of 10 nm. At the same concentration and 50 keV energy, the enhancement reduced from 1.38 to 1.29 due to self-absorption when the GNP diameter was increased from 5 nm to 50 nm, and from 1.36 to 1.33 when 10 nm GNPs clustered with 25 GNPs inside the cluster. At clinically relevant concentrations (<5%), the physical dose enhancement was negligible for protons and carbon-ions (<0.5%).

The radiolysis of water following the initial ionization and excitation processes for all three radiation modalities was simulated, for the first time, for a GNP-loaded cell model. At a GNP concentration of 0.1% in weight, one $^{\bullet}OH$ interacted with a GNP per picosecond for 10 eV protons and the time evolution of the G-value started to change. The changes were qualitatively similar for all three modalities and most pronounced for high LET. For a fixed concentration, the G-value of $^{\bullet}OH$ changed most for the smallest (2 nm) GNP diameter. It was more influenced by isolated than by clustered GNPs. The dependency of the G-value on GNP concentration, size and clustering correlates with the average distance between the chemical species and the GNPs. While the actual behavior of chemical species at the surface of gold nanoparticles cannot yet be simulated, our results show that GNPs irradiated with particle beams may induce negligible physical dose enhancement but may interact significantly with radical species created elsewhere in the water environment. In this way, GNPs introduce chemical changes at very low concentrations that could in part explain the enhancement of the biological effect.

Acknowledgments

This work was supported by the National Cancer Institute under R01 CA187003 (TOPAS nBio, a Monte Carlo tool for radiation biology research) and by the German Research Foundation, DFG, with Grant No. RU 2197/1-1.

References

[1]. Zygmanski Piotr and Sajo Erno. Nanoscale radiation transport and clinical beam modeling for gold nanoparticle dose enhanced radiotherapy (GNPT) using X-rays. The British Journal of Radiology, 89(1059):20150200, 2016. [PubMed: 26642305]

[2]. Sotiropoulos Marios, Henthorn Nicholas T., Warmenhoven John W., Mackay Ranald I., Kirkby Karen J., and Merchant Michael J. Modelling direct DNA damage for gold nanoparticle enhanced proton therapy. Nanoscale, 9(46):18413–18422, 2017. [PubMed: 29148554]

[3]. Polf Jerimy C., Bronk Lawrence F., Driessen Wouter H. P., Arap Wadih, Pasqualini Renata, and Gillin Michael. Enhanced relative biological effectiveness of proton radiotherapy in tumor cells with internalized gold nanoparticles. Applied Physics Letters, 98(19):3–5, 2011.

[4]. Li Sha, Penninckx Sébastien, Karmani Linda, Heuskin Anne Catherine, Watillon Kassandra, Marega Riccardo, Zola Jerome, Corvaglia Valentina, Genard Geraldine, Gallez Bernard, Feron Olivier, Martinive Philippe, Bonifazi Davide, Michiels Carine, and Lucas Stéphane. LET-dependent radiosensitization effects of gold nanoparticles for proton irradiation. Nanotechnology, 27(45), 2016.

[5]. Rashid Raizulnasuha Abdul, Abidin Safri Zainal, Anuar Muhammad Afiq Khairil, Tominaga Takahiro, Akasaka Hiroaki, Sasaki Ryohei, Kie Katahira, Razak Khairunisak Abdul, Pham Binh T.T., Hawkett Brian S., Carmichael Mary Ann, Geso Moshi, and Rahman Wan Nordiana. Radiosensitization effects and ROS generation by high Z metallic nanoparticles on human colon carcinoma cell (HCT116) irradiated under 150 MeV proton beam. OpenNano, 4, 2019.

[6]. Peukert Dylan, Kempson Ivan, Douglass Michael, and Bezak Eva. Metallic nanoparticle radiosensitisation of ion radiotherapy: A review. Physica Medica, 47(February):121–128, 2018. [PubMed: 29609813]

[7]. Kuncic Zdenka and Lacombe Sandrine. Nanoparticle radio-enhancement: principles, progress and application to cancer treatment. Physics in Medicine & Biology, 63(2):02TR01, 2018.

[8]. Schuemann Jan, Berbeco Ross, Chithrani Devika B., Cho Sang Hyun, Kumar Rajiv, McMahon Stephen J., Sridhar Srinivas, and Krishnan Sunil. Roadmap to Clinical Use of Gold Nanoparticles for Radiation Sensitization. International Journal of Radiation Oncology, Biology, Physics, 94(1):189–205, 2016. [PubMed: 26700713]

[9]. Rosa Soraia, Connolly Chris, Schettino Giuseppe, Butterworth Karl T., and Prise Kevin M. Biological mechanisms of gold nanoparticle radiosensitization. Cancer Nanotechnology, 8(1), 2017.

[10]. Xie WZ, Friedland W, Li WB, Li CY, Oeh U, Qiu R, Li JL, and Hoeschen C. Simulation on the molecular radiosensitization effect of gold nanoparticles in cells irradiated by x-rays. Physics in Medicine and Biology, 60(16):6195–6212, 2015. [PubMed: 26226203]

[11]. Karamitros M, Luan S, Bernal MA, Allison J, Baldacchino G, Davidkova M, Francis Z, Friedland W, Ivantchenko V, Ivantchenko A, Mantero A, Nieminem P, Santin G, Tran HN, Stepan V, and Incerti S Diffusion-controlled reactions modeling in Geant4-DNA. Journal of Computational Physics, 274:841–882, 2014.

[12]. Boscolo D, Krämer M, Durante M, Fuss MC, and Scifoni E TRAX-CHEM: A pre-chemical and chemical stage extension of the particle track structure code TRAX in water targets. Chemical Physics Letters, 698:11–18, 2018.

[13]. Uehara Shuzo and Nikjoo Hooshang. Monte Carlo simulation of water radiolysis for low-energy charged particles. Journal of radiation research, 47(1):69–81, 2006. [PubMed: 16571920]

[14]. Plante Ianik and Devroye Luc. Considerations for the independent reaction times and step-by-step methods for radiation chemistry simulations. Radiation Physics and Chemistry, 139:157–172, 2017.

[15]. Ramos-Méndez J, Perl J, Schuemann J, McNamara A, Paganetti H, and Faddegon B Monte Carlo simulation of chemistry following radiolysis with TOPAS-nBio. Physics in Medicine & Biology, 63(10):105014, 2018. [PubMed: 29697057]

[16]. Misawa Masaki and Takahashi Junko. Generation of reactive oxygen species induced by gold nanoparticles under x-ray and UV Irradiations. Nanomedicine: Nanotechnology, Biology, and Medicine, 7(5):604–614, 2011. [PubMed: 21333754]

[17]. Sicard-Roselli Cécile, Brun Emilie, Gilles Manon, Baldacchino Gérard, Kelsey Colin, McQuaid Harold, Polin Chris, Wardlow Nathan, and Currell Frederick. A new mechanism for hydroxyl radical production in irradiated nanoparticle solutions. Small, 10(16):3338–3346, 2014. [PubMed: 24863679]

[18]. Seo Seung Jun, Jeon Jae Kun, Han Sung Mi, and Kim Jong Ki. Reactive oxygen species-based measurement of the dependence of the Coulomb nanoradiator effect on proton energy and atomic Z value. International Journal of Radiation Biology, 93(11):1239–1247, 2017. [PubMed: 28752783]

[19]. Pan Yu, Leifert Annika, Ruau David, Neuss Sabine, Bornemann Jörg, Schmid Günter, Brandau Wolfgang, Simon Ulrich, and Jahnen-Dechent Willi. Gold nanoparticles of diameter 1.4 nm trigger necrosis by oxidative stress and mitochondrial damage. Small, 5(18):2067–2076, 2009. [PubMed: 19642089]

[20]. Liu Ru, Wang Yaling, Yuan Qing, An Deyi, Li Jingyuan, and Gao Xueyun. The Au clusters induce tumor cell apoptosis via specifically targeting thioredoxin reductase 1 (TrxR1) and suppressing its activity. Chemical Communications, 50(73):10687–10690, 2014. [PubMed: 25078326]

[21]. Liu Yan, Liu Xi, Jin Xiaodong, He Pengbo, Zheng Xiaogang, Dai Zhongying, Ye Fei, Zhao Ting, Chen Weiqiang, and Li Qiang. The dependence of radiation enhancement effect on the concentration of gold nanoparticles exposed to low- and high-LET radiations. Physica Medica, 31(3):210–218, 2015. [PubMed: 25651760]

[22]. He Weiwei, Zhou Yu Ting, Wamer Wayne G., Hu Xiaona, Wu Xiaochun, Zheng Zhi, Boudreau Mary D., and Yin Jun Jie. Intrinsic catalytic activity of Au nanoparticles with respect to hydrogen peroxide decomposition and superoxide scavenging. Biomaterials, 34(3):765–773, 2013. [PubMed: 23103160]

[23]. Tran HN, Karamitros M, Ivanchenko VN, Guatelli S, McKinnon S, Murakami K, Sasaki T, Okada S, Bordage MC, Francis Z, El Bitar Z, Bernal MA, Shin JI, Lee SB, Barberet Ph, Tran TT, Brown JMC, Nhan Hao TV, and Incerti S Geant4 Monte Carlo simulation of absorbed dose and radiolysis yields enhancement from a gold nanoparticle under MeV proton irradiation. Nuclear Instruments and Methods in Physics Research, Section B: Beam Interactions with Materials and Atoms, 373:126–139, 2016.

[24]. Schuemann J, McNamara AL, Ramos-Méndez J, Perl J, Held KD, Paganetti H, Incerti S, and Faddegon B TOPAS-nBio: An Extension to the TOPAS Simulation Toolkit for Cellular and Sub-cellular Radiobiology. Radiation Research, 000:RR15226.1, 2019.

[25]. McNamara Aimee, Geng Changran, Turner Robert, Mendez Jose Ramos, Perl Joseph, Held Kathryn, Faddegon Bruce, Paganetti Harald, and Schuemann Jan. Validation of the radiobiology toolkit TOPAS-nBio in simple DNA geometries. Physica Medica, 33:207–215, 2017. [PubMed: 28017738]

[26]. Perl J, Shin J, Schümann J, Faddegon B, and Paganetti H TOPAS: An innovative proton Monte Carlo platform for research and clinical applications. Medical Physics, 39(11):6818–6837, 2012. [PubMed: 23127075]

[27]. Incerti S, Baldacchino G, Bernal M, Capra R, Champion C, Francis Z, Guye P, Mantero A, Mascialino B, Moretto P, Nieminen P, Villagrasa C, and Zacharatou C The Geant4-DNA project. International Journal of Modeling, Simulation, and Scientific Computing, 01(02):157–178, 2010.

[28]. Ma Ningning, Wu Fu Gen, Zhang Xiaodong, Jiang Yao Wen, Jia Hao Ran, Wang Hong Yin, Li Yan Hong, Liu Peidang, Gu Ning, and Chen Zhan. Shape-Dependent Radiosensitization Effect of Gold Nanostructures in Cancer Radiotherapy: Comparison of Gold Nanoparticles, Nanospikes, and Nanorods. ACS Applied Materials and Interfaces, 9(15):13037–13048, 2017. [PubMed: 28338323]

[29]. Peckys Diana B. and Jonge Niels De. Visualizing gold nanoparticle uptake in live cells with liquid scanning transmission electron microscopy. Nano Letters, 11(4):1733–1738, 2011. [PubMed: 21410218]

[30]. Chithrani Basnagge Devika, Ghazani Arezou A, and Chan Warren C W. Determining the Size and Shape Dependence of Gold Nanoparticle Uptake into Mammalian Cells. Nano Letters, 6(4):662–668, 2006. [PubMed: 16608261]

[31]. Coulter Jonathan. Cell type-dependent uptake, localization, and cytotoxicity of 1.9 nm gold nanoparticles. International Journal of Nanomedicine, 7(2012):2673, 2012. [PubMed: 22701316]

[32]. Saroori Alexander Al, Biswas Abin, Bach Margund, Moser Felipe, Hildenbrand Georg, Mu Patrick, Wenz Frederik, Cremer Christoph, Burger Nina, Veldwijk Marlon R., Hausmann Michael, Müller Patrick, Saroori Alexander Al, Biswas Abin, Bach Margund, Wenz Frederik, Cremer Christoph, Burger Nina, Veldwijk Marlon R., Hausmann Michael, Saroori Alexander Al, Biswas Abin, Bach Margund, Moser Felipe, Hildenbrand Georg, Mu Patrick, Wenz Frederik, Cremer Christoph, Burger Nina, Veldwijk Marlon R., and Hausmann Michael. Cellular Uptake of Gold Nanoparticles and Their Behavior as Labels for Localization Microscopy. Biophysical Journal, 110(4):947–953, 2016. [PubMed: 26910431]

[33]. Zygmanski Piotr, Liu Bo, Tsiamas Panagiotis, Cifter Fulya, Petersheim Markus, Hesser Jürgen, and Sajo Erno. Dependence of Monte Carlo microdosimetric computations on the simulation geometry of gold nanoparticles. Physics in medicine and biology, 58(22):7961–77, 2013. [PubMed: 24169737]

[34]. Sakata D, Incerti S, Bordage MC, Lampe N, Okada S, Emfietzoglou D, Kyriakou I, Murakami K, Sasaki T, Tran H, Guatelli S, and Ivantchenko VN An implementation of discrete electron transport models for gold in the Geant4 simulation toolkit. Journal of Applied Physics, 120(24):244901, 2016.

[35]. Lazarakis P, Incerti S, Ivanchenko V, Kyriakou I, Emfietzoglou D, Corde S, Rosenfeld AB, Lerch M, Tehei M, and Guatelli S Investigation of track structure and condensed history physics models for applications in radiation dosimetry on a micro and nano scale in Geant4. Biomedical Physics and Engineering Express, 4(2), 2018.

[36]. Incerti S, Suerfu B, Xu J, Ivantchenko V, Mantero A, Brown JMC, Bernal MA, Francis Z, Karamitros M, and Tran HN Simulation of Auger electron emission from nanometer-size gold targets using the Geant4 Monte Carlo simulation toolkit. Nuclear Instruments and Methods in Physics Research, Section B: Beam Interactions with Materials and Atoms, 372:91–101, 2016.

[37]. Meesungnoen Jintana, Jay-Gerin Jean-Paul, Filali-Mouhim Abdelali, Mankhetkorn Samlee, and Carlo Monte. Low-energy electron penetration range in liquid water. Radiation research, 158(5):657–660, 2014.

[38]. Lin Yuting, McMahon Stephen J., Paganetti Harald, and Schuemann Jan. Biological modeling of gold nanoparticle enhanced radiotherapy for proton therapy. Physics in Medicine and Biology, 60(10):4149–4168, 2015. [PubMed: 25953956]

[39]. Sotiropoulos Marios, Taylor Michael, Henthorn Nicholas, Warmenhoven John, Mackay RI, Kirkby KJ, and Merchant Michael. Geant4 interaction model comparison for dose deposition from gold nanoparticles under proton irradiation. Biomedical Physics & Engineering Express, 3, 2017.

[40]. Hubbell JH and Seltzer SM NIST Standard Reference Database 126. Technical report, Radiation Physics Division, PML, NIST, 1996.

[41]. Williams G Thompson A, Attwood D, Gullikson E, Howells M, Kim K-J, Kirz J, Kortright J, Lindau I, Liu Y, Pianetta P, Robinson A, Scofield J, Underwood J X-Ray Data Booklet. Lawrence Berkeley National Laboratory, 2009.

[42]. Bernal M. a. and Liendo J. a. The HKS model for electron production in liquid water by light ions. Nuclear Instruments and Methods in Physics Research, Section B: Beam Interactions with Materials and Atoms, 251(1):171–176, 2006.

[43]. Wälzlein C, Scifoni E, Krämer M, and Durante M. Simulations of dose enhancement for heavy atom nanoparticles irradiated by protons. Physics in Medicine and Biology, 59(6):1441–1458, 2014. [PubMed: 24584098]

[44]. Hespeels Félicien, Lucas Stephane, Tabarrant Tijani, Scifoni Emanuele, Kraemer Michael, Chêne Gregoire, Strivay David, Tran Hoang N, and Heuskin AC. Experimental measurements validate

the use of the binary encounter approximation model to accurately compute proton induced dose and radiolysis enhancement from gold nanoparticles. Physics in Medicine & Biology, 64(6):065014, mar 2019. [PubMed: 30731439]

[45]. Sakata Dousatsu, Kyriakou Ioanna, Okada Shogo, Tran Hoang N., Lampe Nathanael, Guatelli Susanna, Bordage Marie Claude, Ivanchenko Vladimir, Murakami Koichi, Sasaki Takashi, Emfietzoglou Dimitris, and Incerti Sebastien. Geant4-DNA track-structure simulations for gold nanoparticles: The importance of electron discrete models in nanometer volumes. Medical Physics, 45(5):2230–2242, 2018. [PubMed: 29480947]

[46]. Gadoue Sherif M., Zygmanski Piotr, and Sajo Erno. The dichotomous nature of dose enhancement by gold nanoparticle aggregates in radiotherapy. Nanomedicine, 13(8):809–823, 2018. [PubMed: 29485321]

[47]. Gadoue Sherif M, Toomeh Dolla, Zygmanski Piotr, and Sajo Erno. Angular dose anisotropy around gold nanoparticles exposed to X-rays. Nanomedicine: Nanotechnology, Biology and Medicine, 13(5):1653–1661, 2017. [PubMed: 28285162]

[48]. Kirkby Charles, Koger Brandon, Suchowerska Natalka, and McKenzie David R. Dosimetric consequences of gold nanoparticle clustering during photon irradiation:. Medical Physics, 44(12):6560–6569, 2017. [PubMed: 28994464]

[49]. Kwon Jihun, Sutherland Kenneth, Makarova Anastasia, Matsuura Taeko, Hashimoto Takayuki, Peng Hao, Toshito Toshiyuki, Umegaki Kikuo, Shirato Hiroki, and Shimizu Shinichi. Investigation of energy absorption by clustered gold nanoparticles. Nuclear Instruments and Methods in Physics Research, Section B: Beam Interactions with Materials and Atoms, 429(December 2017):34–41, 2018.

[50]. Chelnokov E, Cuba V, Simeone D, Guigner JM, Schmidhammer U, Mostafavi M, and Le Caër S Electron transfer at oxide/water interfaces induced by ionizing radiation. Journal of Physical Chemistry C, 118(15):7865–7873, 2014.

[51]. Cheng Neal N., Starkewolf Zane, Andrew Davidson R, Sharmah Arjun, Lee Changju, Lien Jennifer, and Guo Ting. Chemical enhancement by nanomaterials under X-ray irradiation. Journal of the American Chemical Society, 134(4):1950–1953, 2012. [PubMed: 22260210]

[52]. McNamara AL, Kam WWY, Scales N, McMahon SJ, Bennett JW, Byrne HL, Schuemann J, Paganetti H, Banati R, and Kuncic Z. Dose enhancement effects to the nucleus and mitochondria from gold nanoparticles in the cytosol. Physics in Medicine and Biology, 61(16):5993–6010, 2016. [PubMed: 27435339]

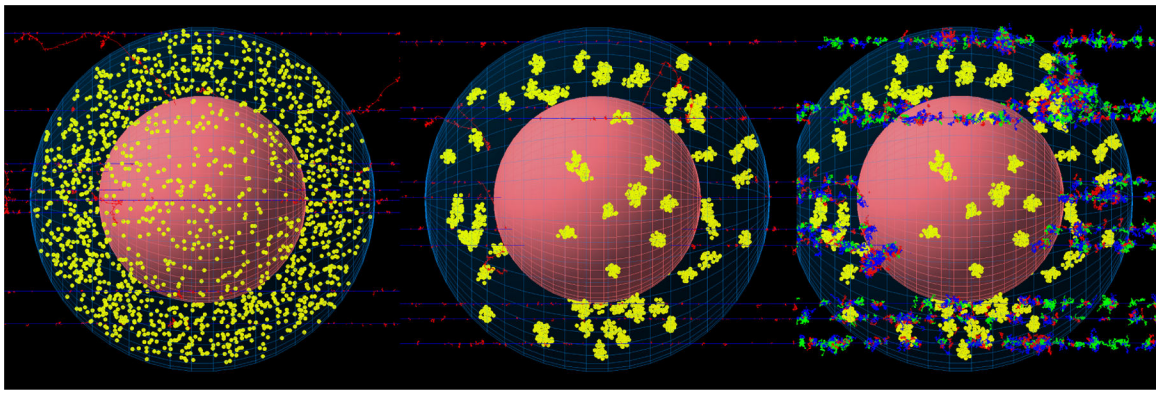

Figure 1.

Small cell model (0.9 μm diameter) used for proton and carbon-ion simulations; the model used for photons is ten times larger. The GNP diameter is 10 nm, the concentration is 5% in weight and all GNPs are distributed withing the cytoplasm either isolated (left) or clustered in groups of 25 GNPs (middle and right). The nucleus (0.54 μm diameter) is shown in red. Tracks of ten 10 MeV protons are are drawn in blue and secondary electrons in red. The right picture shows the diffusion of radiolysis products after 10 ns.

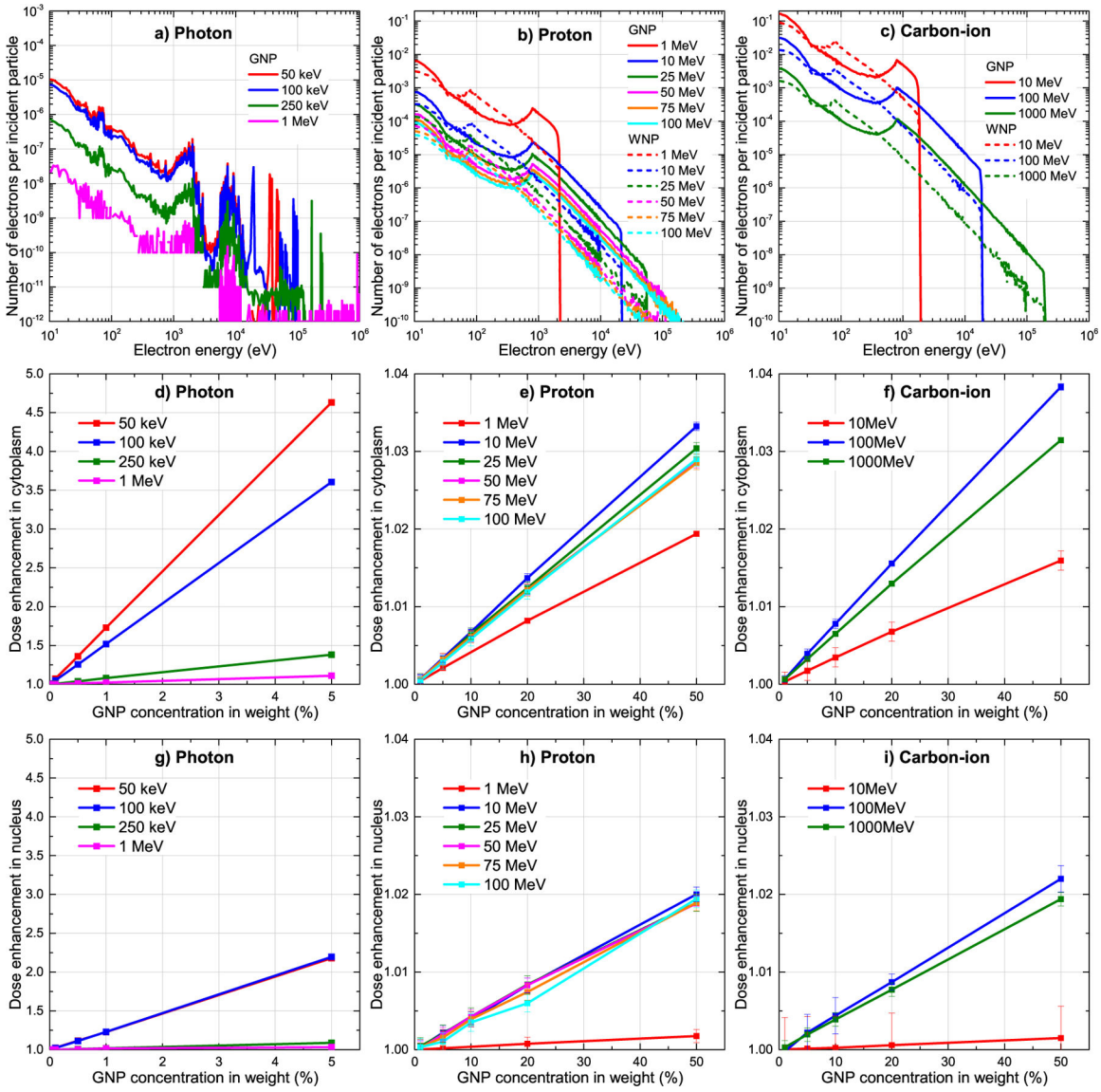

Figure 2.

Energy spectra on the surface of a 10 nm GNP (solid lines) and WNP (light colors, dotted lines) for a) photon, b) proton and c) carbon-ion beams of various energies. Dose enhancement in the cytoplasm (d, e, f) and nucleus (g, h, i) as a function of GNP concentration. Note that the GNP concentration is up to 5% for photons but up to 50% for protons and carbon-ions. The error bars indicate the statistical uncertainty in form of one standard deviation.

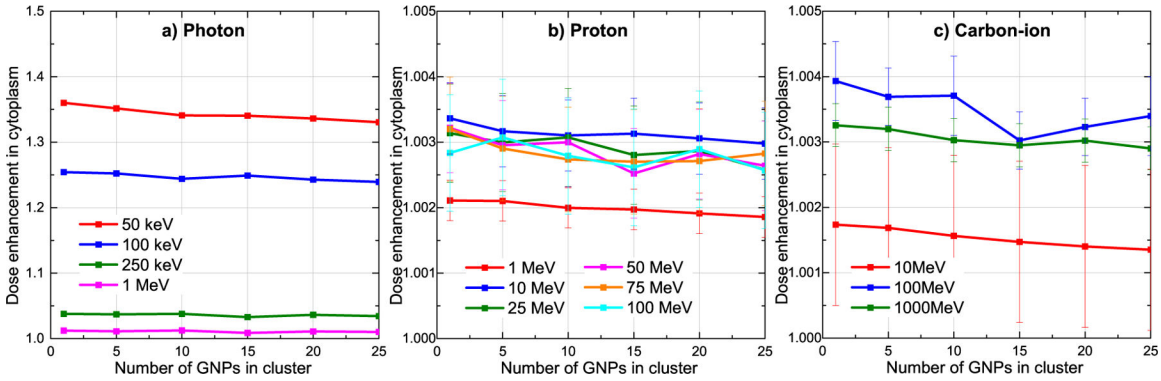

Figure 3.

Dose enhancement in the cytoplasm as a function of GNP clustering for photons, protons and carbon-ions of various energies. The GNP diameter is 10 nm and the concentration in weight is 0.5% for photons and 5% for protons and carbon-ions. The error bars indicate the statistical uncertainty.

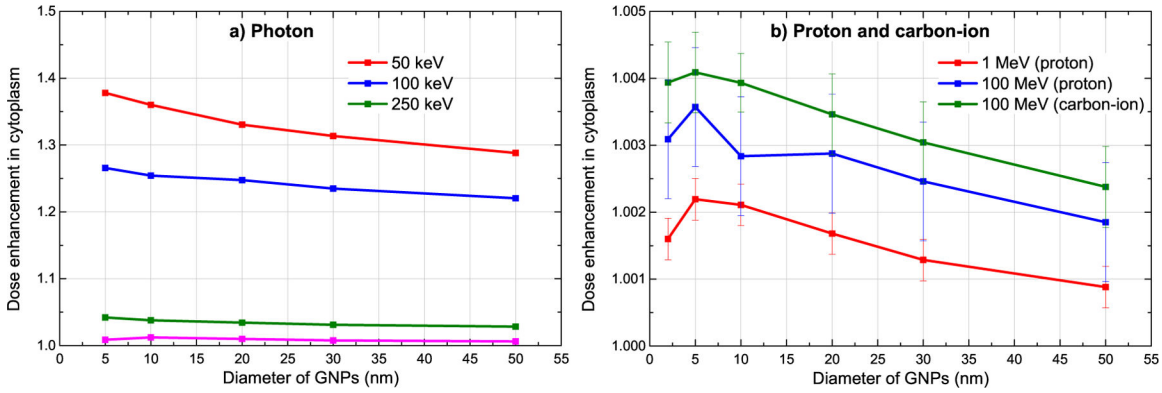

Figure 4.

Dose enhancement in the cytoplasm as a function of GNP size for photons, protons and carbon-ions of various energies. The GNPs are not clustered. The concentration in weight is 0.5% for photons and 5% for protons and carbon-ions. The error bars indicate the statistical uncertainty in form of one standard deviation.

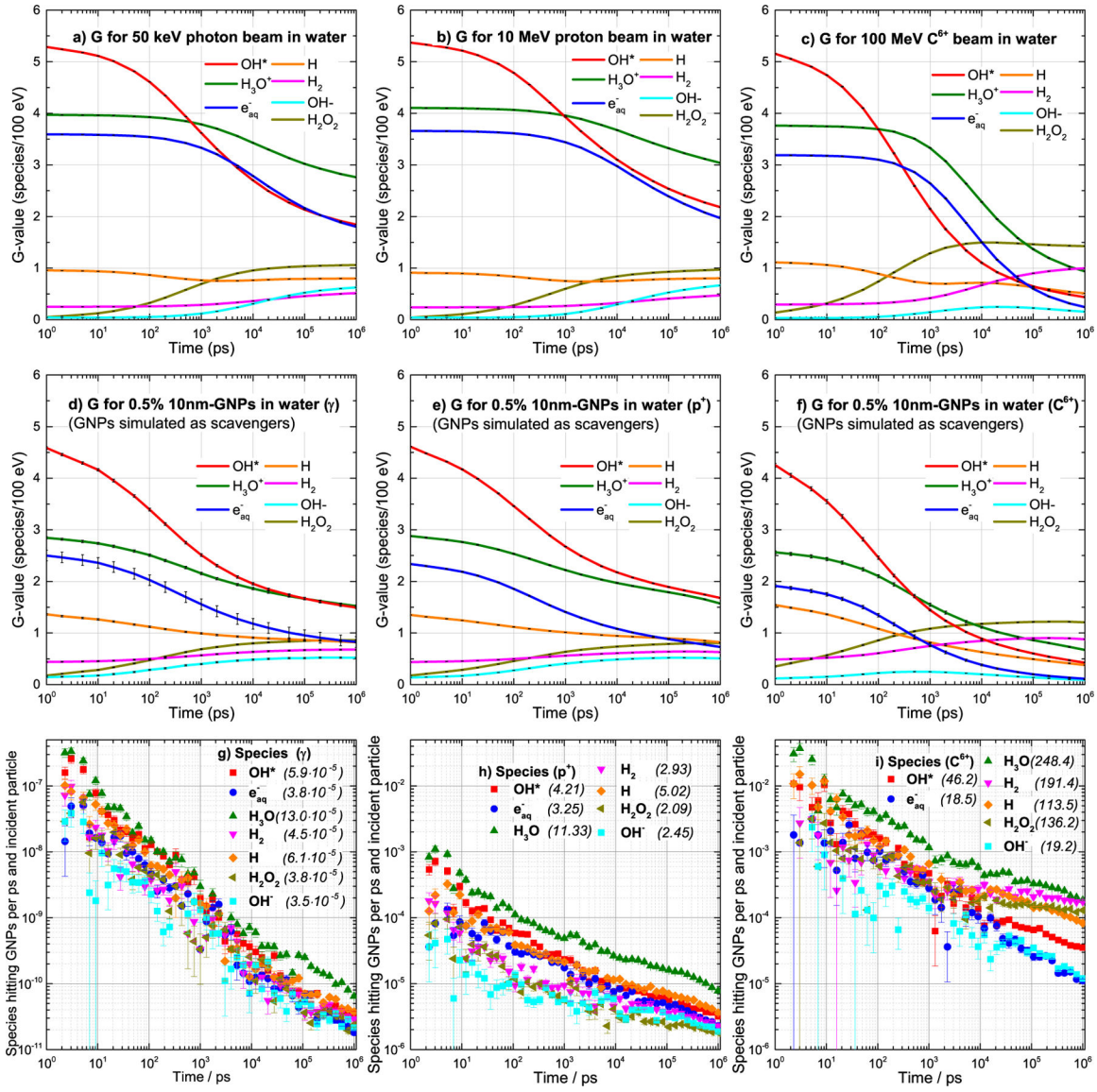

Figure 5.

Temporal evolution of the G-value for all seven radical species generated by a) a 50 keV photon beam, b) a 10 MeV proton beam and c) a 100 MeV carbon-ion beam in the small water-filled cell model. The sub-figures d), e) and f) show G-values for the same radiation modalities and the model filled with 0.5% 10 nm large GNPs in the cytoplasm. Radical species are terminated in the simulation once they hit a GNP. The number of radicals hitting the GNPs per picosecond is displayed in subfigures g), h) and i). These numbers are normalized on the number of incident particles; note that the scale of the y-axis is five orders of magnitude smaller for incident photons than for the particle beams.

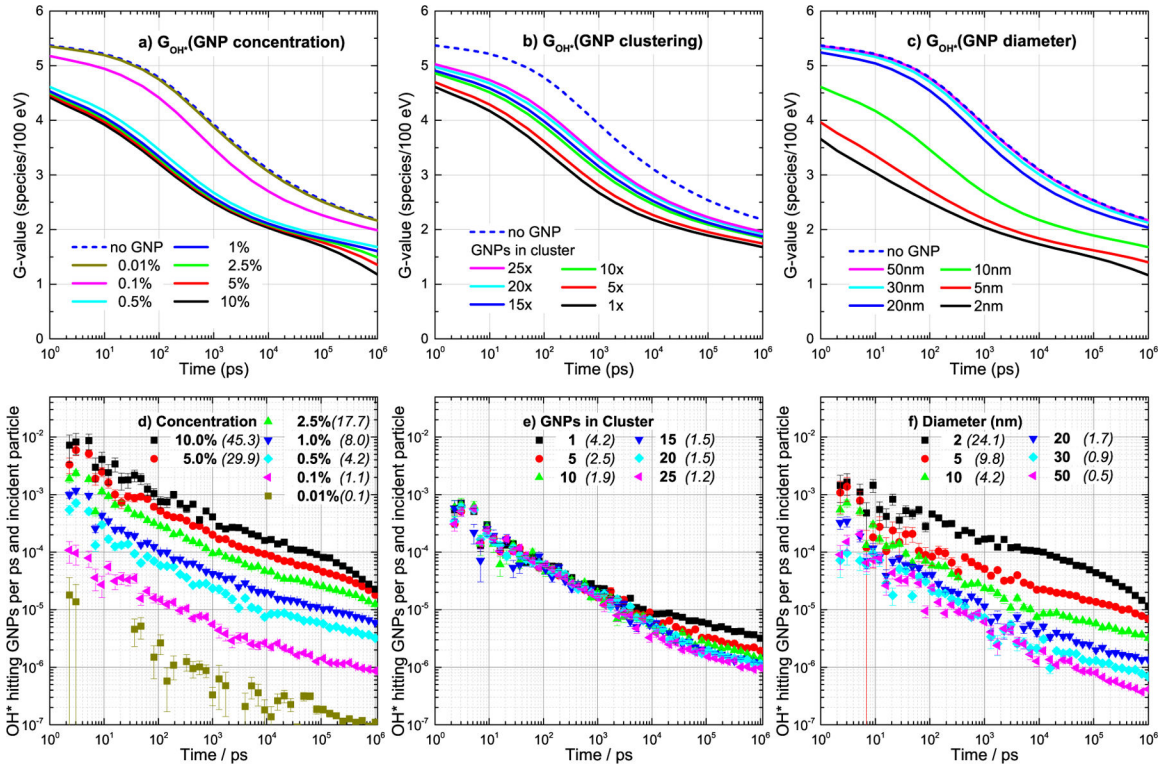

Figure 6.

Temporal evolution of the G-value for the hydroxyl radical $OH^{\bullet}$ for various a) GNP concentrations, b) number of GNPs within a cluster, and c) GNP diameters. The blue dashed line is the reference for a cell volume without GNPs. The following sub-figures d), e), and f) show the number of hydroxyl radicals $OH^{\bullet}$ hitting GNPs in the GNP-loaded for the same three variables. The integral for each curve is given in brackets in the legends. Unless otherwise stated, the parameter set comprises a 10 MeV proton beam, 0.5% GNP concentration and isolated GNPs of 10 nm diameter.

Table 1.

Number of 10 nm-diameter GNPs for the full range of concentrations in the large cell (9 μm diameter) and the small cell (0.9 μm diameter) as used for simulations with photons and with protons and carbon-ions, respectively.

In Weight	In Volume	Mass/Volume	Molar	number of GNPs	
%	%	mg/ml	μM=μmol/l	large	small
50.000	2.588	500	2.61E+06		18866
20.000	1.035	200	1.03E+06		7547
10.000	0.518	100	5.10E+05		3773
5.000	0.259	50	2.54E+05	1886646	1887
1.000	0.052	10	5.08E+04	377329	377
0.500	0.026	5	2.54E+04	188665	189
0.100	0.005	1	5.08E+03	37733	38
0.010	0.001	0.1	5.08E+02	3773	4
0.001	0.000	0.01	5.08E+01	377	

Table 2.

Average distances and minimum diffusion time of randomly distributed chemical species to randomly, homogeneously distributed nanoparticles of various sizes (at concentration of 0.5%) and concentrations (at a diameter of 10 nm).

diameter / nm	NPs	distance /nm	time/ns	surface area /m^2
2	23583	7	3.4	2.96E-13
5	1509	17	21.5	1.19E-13
10	189	34	85.8	5.94E-14
20	24	67	339.3	3.02E-14
30	7	101	772.1	1.98E-14
50	2	152	1754.2	1.57E-14
concentration	**NPs**	**distance /nm**	**time/ns**	**surface area /m^2**
10.00%	3773	11	8.9	1.19E-12
5.00%	1887	14	15.5	5.93E-13
2.50%	943	19	26.4	2.96E-13
1.00%	377	26	52.1	1.18E-13
0.50%	189	34	85.8	5.94E-14
0.10%	38	59	265.6	1.19E-14
0.01%	4	128	1245.0	1.26E-15

Table 3.

Dose enhancement (DE) in the cytoplasm.

Photon energy keV	DE 0.5% conc.	μ_{en}/ρ ratio Au/H_2O	Proton energy MeV	DE 5% conc.	Carbon energy MeV	DE 5% conc.
50	1.36	1.30	1	1.002	1	1.002
100	1.24	1.17	10	1.003	10	1.004
250	1.04	1.01	25	1.003	100	1.003
999	1.01	1.00	50	1.003		
			75	1.003		
			100	1.003		